Journal of Nuclear Materials 377 (2008) 34–40

Contents lists available at ScienceDirect

Journal of Nuclear Materials

journal homepage: www.elsevier.com/locate/jnucmat

Development of ultra-fine grained W–(0.25–0.8)wt%TiC and its superior resistance to neutron and 3 MeV He-ion irradiations

H. Kurishita [a,*], S. Kobayashi [b], K. Nakai [b], T. Ogawa [c], A. Hasegawa [c], K. Abe [c], H. Arakawa [a], S. Matsuo [a], T. Takida [d], K. Takebe [d], M. Kawai [e], N. Yoshida [f]

[a] International Research Center for Nuclear Materials Science, Institute for Materials Research (IMR), Tohoku University, Oarai, Ibaraki 311-1313, Japan
[b] Department of Materials Science and Biotechnology, Ehime University, Matsuyama 790-8577, Japan
[c] Department of Quantum Science and Energy Engineering, Tohoku University, Sendai 980-8579, Japan
[d] A. L. M. T. Corporation, 2 Iwase-koshi-machi, Toyama 931-8543, Japan
[e] Institute of Material Structure Science, High Energy Accelerator Research Organization (KEK), Tsukuba-shi, Ibaraki 305-0801, Japan
[f] Institute for Applied Mechanics, Kyushu University, Kasuga, Fukuoka 816-8580, Japan

A B S T R A C T

W–(0.25–0.8)wt%TiC with equiaxed grain sizes of 50–200 nm and nearly full density of 99% was fabricated utilizing mechanical alloying (MA) in different gas atmospheres of H_2, Ar and N_2 and hot isostatic pressing. Microstructural and mechanical property examinations were conducted before and after irradiations with neutrons at 600 °C to 2×10^{24} n/m^2 and 3 MeV He-ions at 550 °C to 2×10^{23} He/m^2. It is found that TiC additions and MA atmospheres significantly affect grain refinement and baseline mechanical properties. The room-temperature fracture strength takes a maximum of 2 GPa for W–(0.25–0.5)%TiC with MA in H_2 (W–(0.25–0.5)TiC–H_2). At 1400–1700 °C superplastic behavior occurs for W–0.5TiC–H_2, but is suppressed for W–0.5TiC–Ar. No neutron irradiation hardening is recognized in W–0.5TiC–H_2 and W–0.5TiC–Ar. The critical fluence for surface exfoliation by He irradiation for W–0.3TiC–H_2 is more than 10 times as large as that for commercially available W materials. These results suggest that ultra-fine grained W–TiC is capable of improved performance as the spallation neutron source solid target.

1. Introduction

Tungsten (W) is extensively used as a spallation neutron source solid target because of its large mass number, high density, reduced radio activation, good thermal conductivity, low thermal expansion coefficients, etc [1,2]. However, it undergoes serious embrittlement in several regimes, i.e., low temperature embrittlement, recrystallization embrittlement and radiation embrittlement. In order to achieve high performance of W as the spallation neutron source solid target, it is required to significantly mitigate such embrittlement, especially degradation by high-energy particle irradiation. Extensive studies of radiation effects on W and its alloys were made [3–12]. It was shown that there are three possible methodologies for the reduction of degradation due to irradiation, i.e., utilization of radiation-induced intergranular precipitation [9,13–15], radiation-induced phase transformation (intrinsic martensite formation) [16,17] and introduction of a very high density of sinks for irradiation induced point defects.

The introduction of a very high density of sinks will be of the most significance among the methodologies because it can cover the other two methodologies providing that the purity is high in the fine grains [16,17] and the dislocation density is low [18] and can thus offer preferable influences over wide irradiation conditions. However, application of this methodology to W material development resulted in less densification (relative density of ~94% [8,9]) and completely brittle fracture at low stresses even prior to irradiation.

Advanced powder metallurgical methods [12,19,20] utilizing mechanical alloying (MA) [21] and hot isostatic pressing (HIP) processes enabled to produce W–(0.3–0.7)wt%TiC with the average grain size of 50–200 nm and a relative density of approximately 99% [12,20,22], which is referred to as ultra-fine grained (UFG) W–TiC. Such UFG W–TiC consolidates exhibited a maximum fracture strength of approximately 2 GPa at room temperature [12,22]. However, the maximum fracture strength is still below the yield strength of UFG W–TiC and no ductility is assured prior to fracture. The assurance of room-temperature ductility hence remains to be accomplished for UFG W–TiC.

A noted finding regarding this respect is that plastic working after consolidation significantly increases the fracture strength accompanied with appreciable room-temperature ductility and the ductility increase becomes prominent with decreasing grain size from 2 to 0.6 μm [12,19,20]. Therefore, the above main problem is expected to be overcome by applying a sufficient degree of plastic working without a significant change in the UFG

* Corresponding author. Tel.: +81 29 267 4157; fax: +81 29 267 4947.
E-mail address: kurishi@imr.tohoku.ac.jp (H. Kurishita).

0022-3115/$ - see front matter © 2008 Elsevier B.V. All rights reserved.
doi:10.1016/j.jnucmat.2008.02.055

structures (grain size: 50–200 nm) to less-workable W–TiC consolidates. The UFG structures are known to exhibit superplasticity. Superplastic deformation can be utilized as a plastic working process for less-workable W–TiC consolidates and thus it is important to reveal high temperature deformation of UFG W–TiC in connection with superplasticity.

Regarding radiation resistance of W–TiC, on the other hand, it was shown that fine-grained W–0.3TiC (grain size: 0.9 μm) exhibits higher resistance to neutron irradiation at 290 °C to 9×10^{23}n/m^2 ($E > 1$ MeV) than commercially available pure W [12]. However there are no reports on the effects of neutron/He-ion irradiations for UFG W–TiC with grain sizes of 50–200 nm.

In this paper, the current status of UFG W–TiC development will be presented, including the features of microstructures and mechanical properties at room and high temperatures in the unirradiated state. Effects of irradiation with neutrons or 3 MeV helium-ions on microstructures and room temperature mechanical properties will be also presented.

2. Experimental

Powders of pure tungsten (an average particle size 4.0 μm and purity 99.9%) and TiC (40 μm, 99.9%) were mixed to provide nominal compositions of W, W–0.25TiC, W–0.3TiC, W–0.5TiC, W–0.7TiC, W–0.8TiC (in wt%) in a glove box and then charged into two vessels made of TZM together with TZM balls for MA. MA treatments were conducted by a 3 MPDA (three mutually perpendicular direction agitation) ball mill in a purified H_2 (purity 99.99999%), Ar or N_2 gas atmosphere. The details of the MA processes are reported elsewhere [8,9,19,20].

The MA treated powder was degassed and then charged into a mild steel capsule and then subjected to HIP in an Ar atmosphere at 1350 °C and 200 MPa for 10.8 ks. The dimensions of the as-HIPed compacts were approximately 25 mm in diameter and 26 mm in height. The measured relative densities of the as-HIPed compacts were in a range of 98.8–99.4%, with a less densification for W–TiC consolidates with MA in Ar. The contents of oxygen and nitrogen impurities in the W–TiC compacts with MA in purified H_2 and Ar were approximately 200–400 and 60–100 wppm, respectively. The Mo contents arising from the TZM vessels and balls during MA were in a range between 1.7 and 2.6 wt%. These impurity contents were slightly higher for W–TiC with MA in H_2 than for that in Ar. Hereafter, W–TiC compacts fabricated with a H_2 or Ar atmosphere for milling is called W–TiC–H_2 or W–TiC–Ar.

Thin foils for transmission electron microscopy (TEM) observations were prepared by twin-jet electropolishing using a solution of 20 vol.% H_2SO_4 and 80 vol.% C_2H_5OH around 5 °C at 20 V. They were subjected to TEM microstructural examinations and EDX analyses using a JEM-2000FX and JEM-4000FX operating at 200 and 400 kV, respectively.

Miniaturized specimens for three-point bend (3PB) and tensile tests were machined with the dimensions of 1 mm by 1 mm by 20 mm and the gage sections of 1.2 mm by 0.5 mm by 5 mm [23], respectively, and mechanically polished with emery disks up to #1500. 3PB tests were conducted at room temperature with a span of 13.3 mm and a crosshead speed of 0.01 mm/s using a servo-hydraulic fatigue testing machine (Shimadzu Servopulser of 50-kN capacity equipped with a 5-kN shear-type load cell). Tensile tests were performed also at temperatures from 1400 to 1700 °C at initial strain rates of 5×10^{-5} to 5×10^{-3} s^{-1} in a vacuum better than 3×10^{-4} Pa with Ta foils used for additional protection of the specimens from pick-up of gaseous impurities during the test. Details of the tests were reported elsewhere [24]. Vickers microhardness measurements were conducted at room temperature with a load of 4.90 N for 20 s for TEM disks or 3PB specimens.

Table 1
3 MeV He irradiation conditions

Accelerated ion	$^4He^+$
Accelerated voltage	3 MeV
Irradiation temperature	823 ± 10 K
Vacuum	~10^{-6} Torr
Beam current	2.0–2.5 μA
Fluence	10^{22}–10^{23} He/m^2

Table 2
Main results of 3 MeV He irradiation tests for four kinds of tungsten materials

Designation	State	Average grain size (μm)	He fluence (He/m^2)	Exfoliation or surface cracks
Pure W/R	Recrystallized	30 × 20	1.8×10^{22}	Yes
K-doped W/R	Recrystallized	50 × 30	2.3×10^{22}	Yes
K-doped W/SR	Stress-relieved	<10	2.6×10^{22}	Yes
W–0.3TiC–H_2	As-HIP	0.19	2.3×10^{23}	No

Fracture surfaces of the tested specimens were examined with a field emission scanning electron microscope (FE/SEM).

Neutron irradiation was performed in a helium atmosphere to a fluence of 2×10^{24} n/m^2 at 600 °C in the Japan Materials Testing Reactor (JMTR). For comparison, TEM disks of commercially available pure W with a grain size of approximately 10 μm in the hot-rolled, stress-relieved condition [12] were also prepared and examined.

He irradiation was conducted by a dynamitron type accelerator at Tohoku University under conditions listed in Table 1. Four kinds of materials were employed for this study (see Table 2), the sample dimensions being 3 mm in diameter and 0.3 mm thickness. The materials of pure W, K-doped W/R and K-doped W/SR are commercially available and were fabricated by A.L.M.T Corporation.

3. Results and discussion

3.1. Microstructures of UFG W–TiC

Fig. 1 shows TEM bright field images for as-HIPed W–0.5TiC–H_2, W–0.5TiC–Ar and W–0.7TiC–H_2, depicting the effects of TiC addition and MA atmosphere on grain structures. The average grain diameter and relative density (the measured density/theoretical density of the as-HIPed consolidates) are indicated. UFG W–TiC consists of equiaxed grains, and TiC addition leads to grain refinement. In particular, MA in an Ar atmosphere has a significant grain refinement effect and leads to a slightly less densification.

Fig. 2 shows a TEM bright-field image and an EDX result for W–0.5TiC–Ar. A large number of nano-size white dots are observed (the number density: $3 \times 10^4/\mu m^3$) and Ar is detected from the observed area.

In view of the EDX result and the results that white dots were not observed in W–(0.3–0.7)TiC–H_2, they are regarded as Ar-contained bubbles. It is most likely that such bubbles give a pinning effect similar to fine dispersoids and cause additional grain refinement.

3.2. Room-temperature mechanical properties of UFG W–TiC

Fig. 3 shows the relationship between Vickers microhardness and average grain diameter for UFG W–TiC. The hardness of UFG W–TiC is in a range of 900–1160 HV and is mainly governed by grain size (grain size strengthening).

Fig. 4 shows the effects of TiC addition and MA atmosphere on 3PB fracture strength. The fracture strength, σ_f, was evaluated by

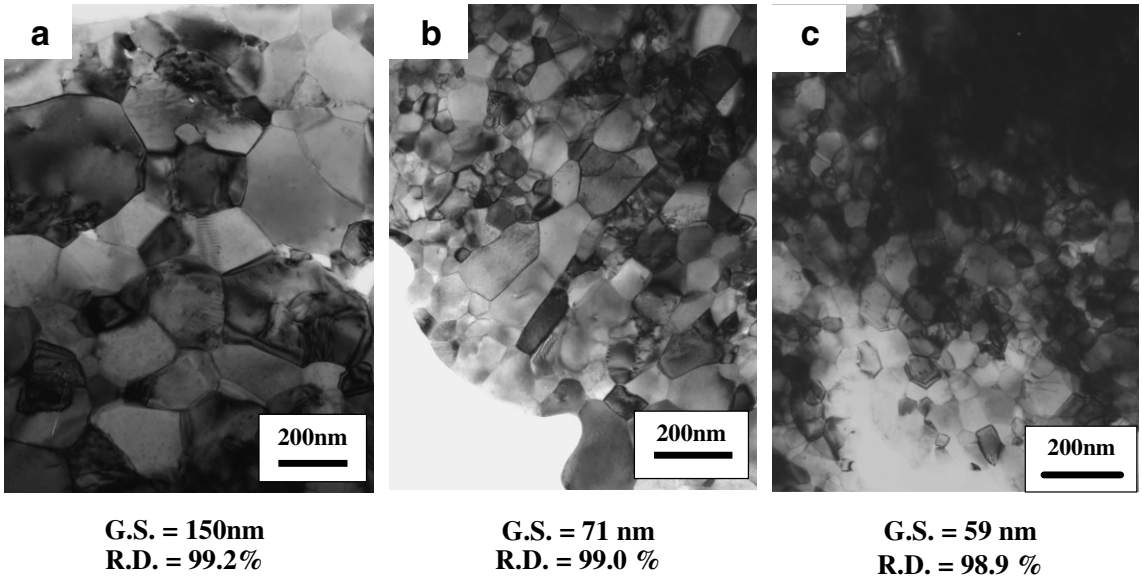

Fig. 1. TEM bright field images showing grain structures of (a) W–0.5TiC–H_2, (b) W–0.5TiC–Ar, (c) W–0.7TiC–Ar.

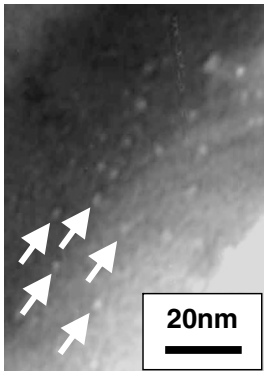

	at%
W	97.30
Ti	0.86
Mo	1.07
Ar	0.77

Fig. 2. TEM bright-field image and an EDX result for W–0.5TiC–Ar.

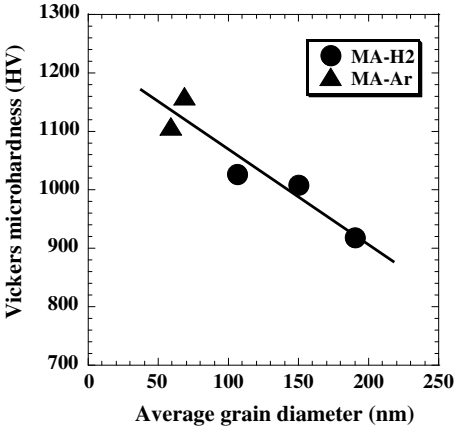

Fig. 3. Relationship between Vickers microhardness and average grain diameter for W–TiC–H_2 and W–TiC–Ar.

$$\sigma_f = 3PL/2Bt^2. \quad (1)$$

Here, P is the applied load, L is the span (13.3 mm), B and t are the specimen width and thickness, respectively. σ_f depends strongly on TiC addition and MA atmosphere: pure W without TiC addition

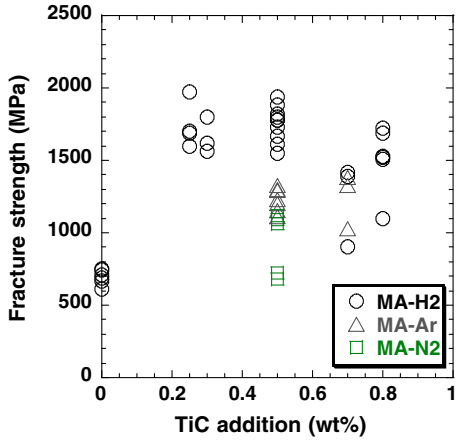

Fig. 4. Effects of TiC addition and MA atmosphere on 3PB fracture strength for W–(0–0.8)TiC with MA in a H_2, Ar or N_2 atmosphere.

(W–H_2) exhibits very low fracture stresses, 630–780 MPa, which are much lower than those for W–TiC–H_2. TiC addition significantly increases σ_f, with a maximum of approximately 2 GPa for (0.25–0.5)TiC additions, however, the dependence of TiC addition from 0.25 to 0.8 wt% on σ_f is not very large. The MA atmosphere increases σ_f in the order of N_2, Ar and H_2. Since the effect of a N_2 atmosphere on σ_f has been shown to be detrimental, in contrast to H_2 and Ar atmospheres, no further examinations were conducted for W–0.5TiC–N_2,

The high strength of UFG W–TiC is attributable to the following microstructural factors: (1) grain-boundary strengthening by TiC dispersoids [8,9,12,25], (2) decreasing the effective size of a weak grain boundary acting as a crack initiator by grain refinement [9], and (3) decreasing detrimental effects of pores on the fracture strength due to easier removal of H_2 than Ar and N_2 from the W–TiC consolidates. Regarding factor (1), TiC dispersoids with sizes less than approximately 150 nm were observed at grain boundaries, their dispersion being essentially the same for W–TiC–H_2 and W–TiC–Ar. For factor (2) the grain size is smaller in W–TiC–Ar than in W–TiC–H_2, as shown previously. Therefore, the observed higher fracture strength of W–TiC–H_2 than W–TiC–Ar and W–TiC–N_2 is

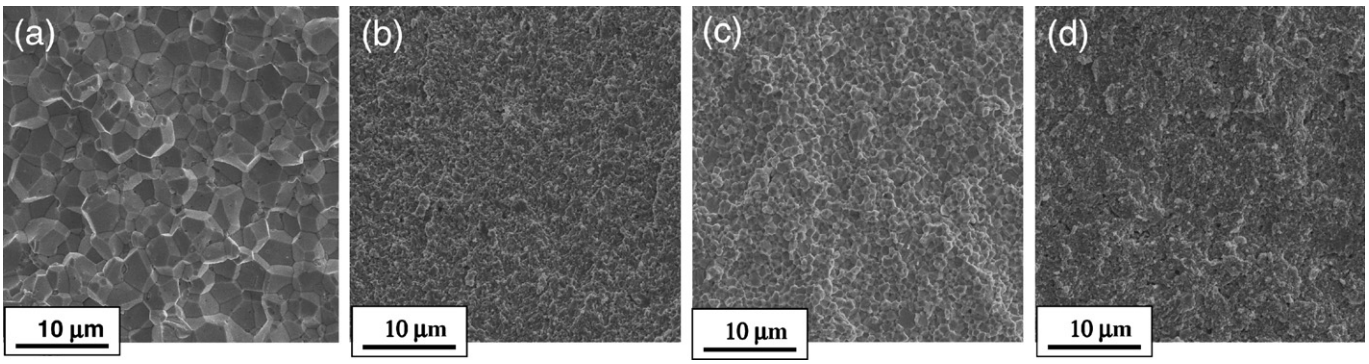

Fig. 5. Fracture surfaces of 3PB tested specimens of (a) pure W–H_2 (σ_f = 0.75 GPa), (b) W–0.25TiC–H_2 (σ_f = 1.97 GPa), (c) W–0.5TiC–H_2 (σ_f = 1.88 GPa) and (d) W–0.8TiC–H_2 (σ_f = 1.72 GPa).

mainly attributed to factor (3), and thorough elimination of gas bubbles and/or pores from UFG W–TiC is the most important issue.

Fig. 5 shows fracture surfaces of bend tested specimen of W–H_2 and W–(0.25–0.8)TiC–H_2, together with each of the measured fracture stresses. W–H_2 exhibits coarse grains due to very high internal energy in MA processed powder introduced by MA and the absence of TiC dispersoids, suffering grain boundary fracture at a very low stress.

Even in the case of W–TiC–H_2, no appreciable ductility occurred prior to fracture. SEM fracture surface examinations of W–0.5TiC–H_2 revealed that the fracture was initiated at coarse grained regions that are identified to be a contaminant TZM fragment arising from the milling balls and vessels during MA [22]. Such TZM fragments were introduced in the late MA stage and were not subjected to sufficient mechanical refining or alloying during MA. Several modifications are in progress to fabricate W–TiC compacts containing negligible amounts of contaminant TZM fragments and less amounts of residual pores.

3.3. High temperature tensile properties

In order to reveal the occurrence of superplastic deformation behavior of UFG W–TiC, the test temperature and strain rate dependences of flow stress were examined for W–0.5TiC–H_2 and W–0.5TiC–Ar. The flow stress is defined here as the stress where the work hardening rate becomes zero and the imposed strain rate is equal to the plastic strain rate. It was shown that both materials exhibit similar temperature dependence of flow stress in the temperature range from 1400 to 1700 °C. On the other hand, the result of strain rate dependence of both materials showed quite different behavior, as shown in Fig. 6. The slope of these straight lines gives the strain rate sensitivity of flow stress, *m*. It should be noted that W–0.5TiC–Ar deformed at 1400 and 1700 °C shows smaller *m* values of 0.2–0.25, while W–0.5TiC–H_2 shows larger *m* values of 0.5–0.6, which is a feature of superplastic materials that should exhibit the strain rate sensitivity over 0.3 [26]. In fact, W–0.5TiC–H_2 was quite uniformly elongated without any cracks above 150%, whereas W–0.5TiC–Ar was able to be elongated up to approximately 60% without necking prior to fracture [27].

In view of the finer grain size in W–0.5TiC–Ar than in W–0.5TiC–H_2 which should enhance grain boundary sliding and thus superplasticity, the difficulty in superplastic deformation for W–0.5TiC–Ar is most likely attributable to the existence of a large number of small Ar bubbles; the bubbles may cause an adverse effect on superplastic deformation. Fracture surface examinations of W–0.5TiC–Ar after the elongation of 55% suggested that Ar bubbles enhance void coalescence and lead to fracture. The details of the high temperature behavior of W–0.5TiC–H_2 and W–TiC–Ar will be reported elsewhere [27].

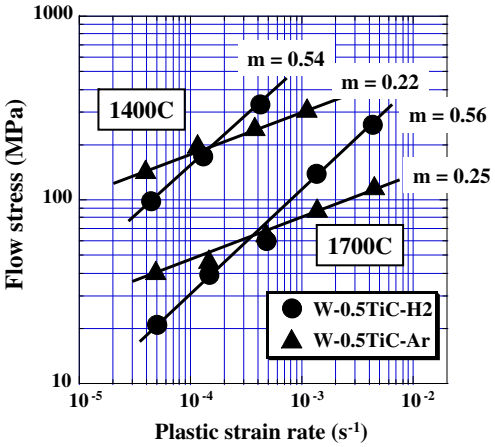

Fig. 6. Strain rate dependence of flow stress at 1673 and 1973 K for W–0.5TiC–H_2 and W–0.5TiC–Ar. *m* is the strain rate sensitivity of flow stress.

3.4. Neutron irradiation effect

Fig. 7 shows TEM bright-field images of microstructures after neutron irradiation for commercially available pure W, W–0.5TiC–H_2 and W–0.5TiC–Ar. A number of irradiation induced defects, such as small black dots or interstitial-type dislocation loops (I-loops), are observed in the grain interior. Fig. 8 shows an enlarged micrograph showing voids in W–0.5TiC–H_2. The number densities of I-loops and voids are listed in Table 3. The number density of voids was obtained by subtracting that of Ar bubbles observed as white dots (Fig. 2). The density of I-loops shows no appreciable difference between the three materials, whereas the density of voids in W–TiC is much smaller than that in pure W and W–0.5TiC–H_2 and W–0.5TiC–Ar exhibit a slight difference in void density. The observed slight difference is attributable to the difference in grain size.

Fig. 9 shows the Vickers microhardness number before and after irradiation for commercially available pure W, W–0.5TiC–H_2 and W–0.5TiC–Ar. The amount of radiation hardening, ΔHV, is 98 for pure W, whereas it is −5 for W−0.5TiC−H_2 and −56 for W–0.5TiC–Ar. This indicates that radiation hardening occurred in pure W, but did not in W–0.5TiC–H_2 and W–0.5TiC–Ar, although the negative values of ΔHV suggest that some recovery of the microstructures introduced in the as-consolidated state occurred during irradiation at 600 °C. In view of the previous results on fine-grained W-0.3TiC and pure W irradiated at 290 °C to 9×10^{23} n/m^2 ($E > 1$ MeV) where ΔHV was 30 for W–0.3TiC and 63 for pure W [12], we can say that the UFG microstructure in W–0.5TiC is very

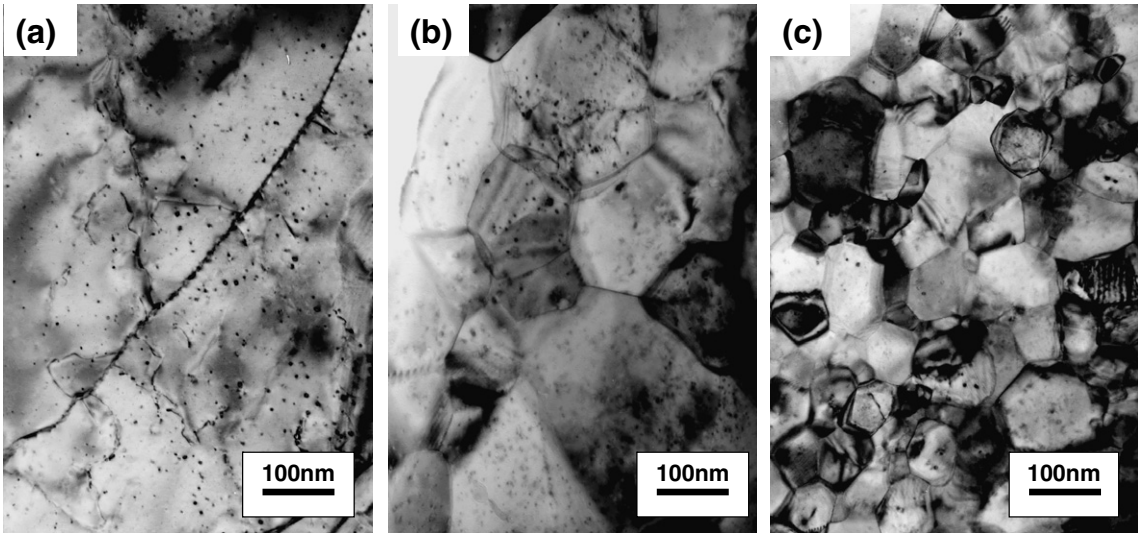

Fig. 7. TEM bright-field images of microstructures in (a) pure W, (b) W–0.5TiC–H_2 and (c) W–0.5TiC–Ar after neutron irradiation at 873K to 2×10^{24} n/m^2 in JMTR.

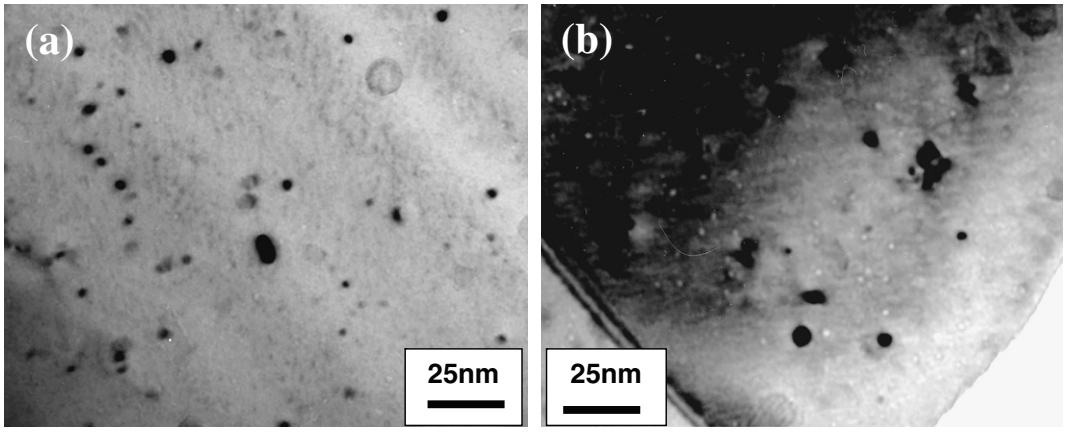

Fig. 8. Enlarged micrographs showing (a) interstitial loops and (b) fine voids in W–0.5TiC–H_2 after neutron irradiation at 873 K to 2×10^{24} n/m^2 in JMTR.

Table 3
Number densities of I-loops and voids in pure W, W–0.5TiC–H_2 and W–0.5TiC–Ar irradiated at 600 °C to 2×10^{24} n/m^2

Number density (N/μm^3)	Pure W	W–0.5TiC–H2	W–0.5TiC–Ar
I-loop	6×10^3	5×10^3	5×10^3
Void	125×10^3	32×10^3	25×10^3

effective in improving the resistance to radiation hardening. In this study no appreciable difference in radiation resistance between W–0.5TiC–H_2 and W–0.5TiC–Ar was recognized.

3.5. He irradiation effect

The four kinds of W materials (pure W/R, K-doped W/R, K-doped W/SR, UFG W–0.3TiC–H_2) were irradiated at 600 °C to different He fluences and their specimen surfaces were observed by optical microscopy. K-doped W is a W material doped with a small amount of Al, K and Si and exhibits high creep resistance [28] and high ductility [29]. The origin of the excellent mechanical properties in the doped-W material is related to an elongated coarse-grained microstructure induced by the additives [30].

The depth-distribution of dpa (displacement per atom) and He concentration caused by 3 MeV He irradiation was calculated with the TRIM code and showed that the dpa and He concentration take a peak around 4–5 μm distant from the original surfaces. It was found that pure W/R, K-doped W/R and K-doped W/SR exhibit exfoliation and surface cracks along grain boundaries after irradiation of about 2×10^{22} He/m^2. An example of such surface cracks is shown in Fig. 10. On the other hand, UFG W–0.3TiC–H_2 exhibited only a few small blisters after irradiation of about 2×10^{22} He/m^2, however it should be noted that the size and number of such

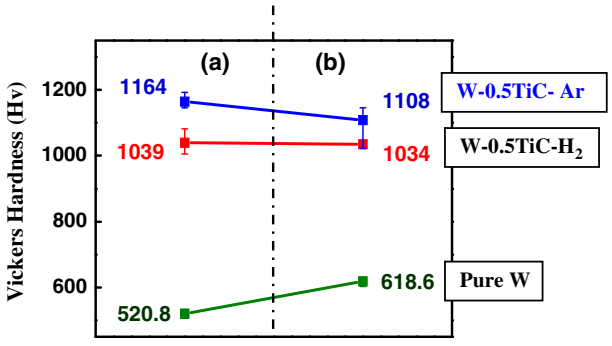

Fig. 9. Vickers microhardness number before and after neutron irradiation for pure W, W–0.5TiC–H_2 and W–0.5TiC–Ar.

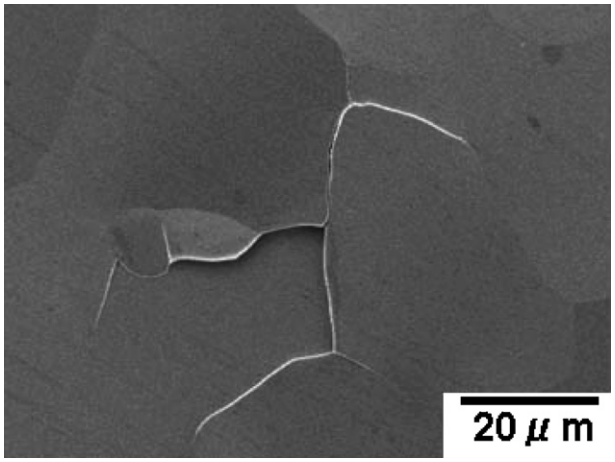

Fig. 10. SEM micrograph of specimen surface after irradiation with 3 MeV He-ions to 1.8×10^{22} He/m^2 for pure W/R.

blisters did not increase and no exfoliation and surface cracks were observed even after irradiation of $2–3 \times 10^{23}$ He/m^2. This indicates that the critical fluence for exfoliation and surface cracks along grain boundaries to occur is about 2×10^{22} He/m^2 for pure W/R, K-doped W/R and K-doped W/SR and is above $2–3 \times 10^{23}$ He/m^2 for UFG W–0.3TiC–H_2. In other words, the surface damage resistance to 3 MeV He irradiations for UFG W–0.3TiC–H_2 is more than 10 times as high as that of the commercially available W materials.

In order to reveal the internal structures after He irradiation, irradiated specimens of K doped W/R and UFG W–0.3TiC–H_2 were cut perpendicularly to the original surfaces by focused ion beam (FIB) techniques and observed by SEM. It was found that for K-doped W/R exfoliation across grain boundaries occurs and the exfoliated face in the blister is relatively smooth, whereas for UFG W–0.3TiC–H_2 a blister presumably due to He accumulation occurs and the exfoliated face in the blister looks very rough. The rugged face of UFG W–0.3TiC–H_2 likely reflects fracture surfaces of individual ultra-fine grains. This suggests that tungsten grain boundaries are essentially capable of accommodating He to some extent and thus an extremely large area of total grain boundaries in UFG W–0.3TiC–H_2 has the beneficial effects of decreasing He concentration per unit area of grain boundaries and suppressing surface damage due to He irradiation.

In order to evaluate radiation hardening by displacement damage and He accumulation caused by 3 MeV He irradiation, Vickers microhardness testing was conducted for the four kinds of W materials before and after He irradiation. The magnitude of radiation hardening decreased in the order of pure W/R, K-doped W/R, K-doped W/SR and UFG W–0.3TiC–H_2, which is in accordance with the order of grain size. It should be noted that the difference in radiation hardening between UFG W–0.3TiC–H_2 and the other three W materials increases with increasing He fluence. This result demonstrates that for these W materials grain boundaries act as the most effective sinks for irradiation produced defects and thus UFG W–0.3TiC–H_2 exhibits higher performance in irradiation environments with the higher He fluence.

4. Conclusions

1. The features of microstructures of UFG W–(0.25–0.8)%TiC are equiaxed grains with average diameters of 50–190 nm and nearly full density of approximately 99%. Significant grain refinement occurs by TiC additions and use of Ar in MA atmosphere which causes a large number of nano-size Ar bubbles in as-HIPed W–TiC consolidates.
2. Vickers microhardness values of UFG W–TiC are in a range of 900–1160 and determined by grain size strengthening.
3. The three-point bend fracture strength at room temperature depends strongly on the TiC addition and MA atmosphere. The strength takes a maximum of approximately 2 GPa for 0.25–0.5TiC additions and increases in the order of N_2, Ar and H_2 as the MA atmosphere, which is mainly attributable to decrease in detrimental effects of pores and/or bubbles due to easier removal of H_2 than Ar and N_2 from the W–TiC consolidates.
4. W–0.5TiC–H_2 exhibits superplastic deformation at 1400–1700 °C, with a larger strain rate sensitivity of flow stress, *m*, of 0.5–0.6. On the other hand, W–0.5TiC–Ar does not exhibit superplastic deformation, with a smaller m value of approximately 0.2. This suggests that the Ar bubbles cause an adverse effect on superplastic deformation.
5. For neutron irradiation to a fluence of 2×10^{24} n/m^2 at 600 °C, W–0.5TiC–H_2 and W–0.5TiC–Ar exhibit no radiation hardening as measured with Vickres microhardness, whereas commercially available pure W shows a considerable hardening of $\Delta HV = 98$. Radiation induced interstitial loops and voids are observed with much less increase in void density for UFG W–0.5TiC than that for commercially available pure W. No significant difference in radiation hardening between the MA atmospheres was recognized under this irradiation condition.
6. The critical fluence for exfoliation and surface cracking along grain boundaries to occur by 3MeV He irradiation at 550 °C is about 2×10^{22} He/m^2 for commercially available W materials (pure W/R, K-doped W/R and K-doped W/SR) and above $2–3 \times 10^{23}$ He/m^2 for UFG W–0.3TiC–H_2. This indicates that surface damage resistance to 3 MeV He irradiations for UFG W–0.3TiC–H_2 is more than 10 times as high as that for the commercially available W materials.

Acknowledgments

The present work was partly supported by Grant-in-Aid for Scientific Research (B) (#19360412), Japan Society for the Promotion of Science (JSPS), which is greatly appreciated.

References

[1] M. Kawai, K. Kikuchi, H. Kurishita, J. Li, M. Furusaka, J. Nucl. Mater. 296 (2001) 312.
[2] M. Kawai, M. Furusaka, K. Kikuchi, H. Kurishita, R. Watanabe, J.-F. Li, K. Sugimoto, T. Yamamura, Y. Hiraoka, K. Abe, A. Hasegawa, M. Yoshiie, N. Takenaka, K. Mishima, Y. Kiyanagi, T. Tanabe, N. Yoshida, T. Igarashi, J. Nucl. Mater. 318 (2003) 38.
[3] J.M. Steichen, J. Nucl. Mater. 60 (1976) 13.
[4] R.K. Williams, F.W. Wiffen, J. Bentley, J.O. Steigler, Metall. Trans. A14 (1983) 655.
[5] P. Krautwasser, H. Derz, E. Kny, High Temp. High Press. 22A (1990) 25.
[6] I.V. Gorynin, V.A. Ignatov, V.V. Rybin, S.A. Fabritsiev, V.A. Kazakov, V.P. Chakin, V.A. Tsykanov, V.R. Barabash, Y.G. Prokofyef, J. Nucl. Mater. 191–194 (1992) 421.
[7] H. Ullmaier, F. Carsughi, Nucl. Instrum. and Meth. B 101 (1995) 406.
[8] Y. Kitsunai, H. Kurishita, M. Narui, H. Kayano, Y. Hiraoka, T. Igarashi, T. Takida, J. Nucl. Mater. 271&272 (1999) 423.
[9] H. Kurishita, Y. Kitsunai, T. Kuwabara, M. Hasegawa, Y. Hiraoka, T. Takida, T. Igarashi, J. Plasma Fusion Res. 75 (1999) 594. in Japanese.
[10] Y. Nemoto, A. Hasegawa, M. Satou, K. Abe, J. Nucl. Mater. 283–287 (2000) 1144.
[11] S.A. Maloy, M.R. James, W. Sommer Jr., G.J. Willcutt Jr., M. Lopez, T.J. Romero, M.B. Toloczko, J. Nucl. Mater. 343 (2005) 219.
[12] H. Kurishita, Y. Amano, S. Kobayashi, K. Nakai, H. Arakawa, Y. Hiraoka, T. Takida, K. Takebe, H. Matsui, J. Nucl. Mater. 367–370 (2007) 1453.
[13] H. Kurishita, Y. Kitsunai, T. Shibayama, H. Kayano, Y. Hiraoka, J. Nucl. Mater. 233–237 (1996) 557.
[14] Y. Kitsunai, H. Kurishita, T. Shibayama, M. Narui, H. Kayano, Y. Hiraoka, J. Nucl. Mater. 239 (1996) 253.
[15] H. Kurishita, OECD (2002) 103.
[16] H. Kurishita, T. Kuwabara, M. Hasegawa, S. Kobayashi, K. Nakai, J. Nucl. Mater. 343 (2005) 318.

[17] H. Kurishita, S. Kobayashi, K. Nakai, T. Kuwabara, M. Hasegawa, J. Nucl. Mater. 358 (2006) 217.
[18] Y. Kitsunai, H. Kurishita, T. Kuwabara, M. Narui, M. Hasegawa, T. Takida, K. Takebe, J. Nucl. Mater. 346 (2005) 233.
[19] Y. Ishijima, H. Kurishita, K. Yubuta, H. Arakawa, M. Hasegawa, Y. Hiraoka, T. Takida, K. Takebe, J. Nucl. Mater. 329–333 (2004) 75.
[20] Y. Ishijima, H. Kurishita, H. Arakawa, M. Hasegawa, Y. Hiraoka, T. Takida, K. Takebe, Mater. Trans. 46 (2005) 568.
[21] J.S. Benjamin, Met. Trans 5 (1970) 2943.
[22] H. Kurishita, S. Kobayashi, K. Nakai, H. Arakawa, S. Matsuo, T. Takida, K. Takebe, M. Kawai, Phys. Scr. T 128 (2007) 76.
[23] T. Kuwabara, H. Kurishita, M. Hasegawa, Mater. Sci. Eng. A 417 (2006) 16.
[24] S. Oda, H. Kurishita, Y. Tsuruoka, S. Kobayashi, K. Nakai, H. Matsui, J. Nucl. Mater. 329–333 (2004) 462.
[25] H. Kurishita, H. Yoshinaga, Mater. Forum 13 (1989) 161.
[26] For instance, J.-P. Poirier, Plasticity at high temperatures in crystalline solids, (Eyrolles, Paris, 1976, Japanese Translation) edited by H. Funakubo, Youkendo, Tokyo, 1980, p. 191.
[27] H. Kurishita, S. Matsuo, H. Arakawa, S. Kobayashi, K. Nakai, T. Takida, K. Takebe, M. Kawai, Mater. Sci. Eng. A 477 (2008) 162.
[28] P.K. Wright, Metall. Trans. A 9 (1978) 955.
[29] E. Pink, K. Sedlatscheck, Metallwissenschaft und Technik 23 (1969) 1249.
[30] D.M. Moon, R.C. Koo, Metall. Trans. 2 (1971) 2115.